Fabrication of high-precision solar filters: variety and limitations.

Yakov Sidorin*, Andrew G. Lunt, Jeff Bergthold, Brandon Keith, and David Lunt
Coronado Technology Group LLC, 1674 S. Research Loop, Ste. 436, Tucson, AZ 85710

ABSTRACT

Using H-alpha etalon-based solar filter as an example, we address the issues of practical realization of etalon-based filters used for solar astronomy and other related applications. The design rationale as well as the choice among two conventional formats of etalons is described, depending on the requirements on the devised solar filter.

Keywords: solar filters, Fabry-Perot etalon, optical contacting, H-alpha.

1. INTRODUCTION

Commercially available multilayer dielectric interference filters can provide high attenuation and spectral transmittance bandwidths as low as 0.2 nm, but for some narrow-band applications – such as solar astronomy - even better spectral selection is needed. Additional appropriate filtering is possible with a single or tandem pair of Fabry-Perot filter etalons (FPEs), which are used as a back-bone of optical filtering systems for direct observing and detection at the solar line of choice (see Table 1, [1]) or in various imaging systems across the visible and near-IR spectrum, for example, as part of spectro-polarimeters [2] or lidar receivers [3,4].

Designation	Wavelength, A	Origin
A	7594	terrestrial oxygen
B	6867	terrestrial oxygen
C	6563	hydrogen ($H\alpha$)
D_1	5896	neutral sodium (*Na I*)
D_2	5890	neutral sodium (*Na I*)
E	5270	neutral iron (*Fe I*)
F	4861	hydrogen ($H\beta$)
H	3968	ionized calcium (*Ca II*)
K	3934	ionized calcium (*Ca II*)

Table 1: Major lines of solar spectrum.

2. LOCATION OF AN ETALON_BASED FILTER WITHIN THE OPTICAL SYSTEM

Positioning of the etalon within the optical system affects the performance of the filter. Two main types of etalon-based filter are conventionally used in both research and amateur astronomy: one is an objective filter (usually accompanied with some secondary filters at the eye-piece end) which is mounted over the front of the telescope, and another is a post-objective filter (usually fitting in the focusing tube of the telescope). In commercial systems, a front-end positioned etalon operates in nearly collimated light (full angle of convergence of about 0.5 degrees) and the peak wavelength varies across the FOV of the etalon-filter according to [11]

* yakov@coronadofilters.com; phone 1 520 760-2431; fax 1 520 624-5083; www.coronadofilters.com

Optical Fabrication, Metrology, and Material Advancements for Telescopes, edited by Eli Atad-Ettedgui, Philippe Dierickx, Proceedings of SPIE Vol. 5494 (SPIE, Bellingham, WA, 2004) · 0277-786X/04/$15 · doi: 10.1117/12.548831

$$\Delta\lambda=\lambda\theta^2/2n^2 \qquad (1)$$

where θ is the half-FOV agle, n is the effective refractive index of the medium inside the cavity. In comparison, the bandwidth of a FPE in a telecentric configuration – when, for example, the etalon is positioned close to the focal point in relatively fast converging beams (F/10 or faster) – broadens across the etalon's field-of-view (FOV) according to [2]

$$\delta\lambda = \left[\left(\frac{\lambda^2(1-R)^2}{2\pi nd\sqrt{R}}\right)^2 + \left(\frac{\lambda^2}{nF_D}\right)^2 + \left(\frac{\lambda\theta^2}{8n}\right)^2\right]^{\backslash 1/2} \qquad (2)$$

(d is the plate separation, R is the reflectance of the etalon mirror) and imperfections of the FPE and its coatings have large effects on the final image quality. Table 2 compares the important trade-offs of the etalons, either solid or air-spaced, which function as optical frequency to intensity filters.

Parameter	Air-spaced Etalons	Solid-spaced Etalons
Pressure Tuning	Yes	No
Temperature Stability	Good [1]	Average
Temperature Tuning	No	Yes
Angular Tuning	Yes	Yes
Dispersion	No	Yes
Fabrication Tolerances	Good	Good
Cost	$$	$
Size	Variable (typically large)	Variable (typically small)
Angular Acceptance	Fixed and Limited	Proportional to effective index of the cavity

[1] the temperature stability of the air-spaced etalon should be defined in transient, i.e. while temperature of the filter is changing, and mostly relates to the issue of maintaining the gap parallel.

Table 2

Hydrogen alpha (or H-alpha) etalon-based filters are specifically designed to isolate the principle wavelength of hydrogen in the solar spectrum to allow observing the Sun's chromosphere. In order to see the details of the chromosphere, the pass-band of these filters must be narrower than 0.1 nm, and all wavelengths other than H-alpha line must be safely suppressed to below well-defined eye-safety levels. To satisfy these requirements, we use precisely designed and implemented combinations of etalons, UV- and IR-blocking filters, as well as appropriately matched narrow-pass-band filters. For example, an energy-rejection filter (ERF) covering the objective reduces the amount of heat and damaging UV light that enters the telescope. A blocking filter (BF) rejects the unwanted orders of the etalon. Key parameters for BFs include steepness of the pass-band edges, bandwidth, and out-of-band rejection. An ideal BF should provide low temperature-dependent spectral drift (less than 0.03 Å/°C), a FOV large enough to operate in relatively fast converging beams, and very low (better than 10^{-5}) transmission out-of-band. In the visible spectral region, we recommend using a durable BF with a FWHM of a few angstroms, built as a multi-cavity interference filter using hard refractory oxide materials and ion-assisted sputtering.

The required resulting spectral performance is characterized by pass-bands below 0.7 A. (see Figs. 1 and 2). Figure 3 demonstrates a typical imaging quality achievable with H-alpha front-end solar filters [6].

3. PARAMETERS AFFECTING THE FINESSE OF THE ETALONS, AND PROVIDED SOLUTIONS

FPEs are extremely sensitive to very small optical defects of reflective surfaces and their mutual positioning, since detrimental effects accumulate through multiple reflections. Surface defects may be characterized by a defect finesse (F_D) which is employed, together with the reflectance finesse (F_R) of the ideal FPE, in a Gaussian approximation to define effective finesse (F_E) of the device:

$$F_E = \left(F_R^{-2} + F_D^{-2}\right)^{-1/2} \tag{3}$$

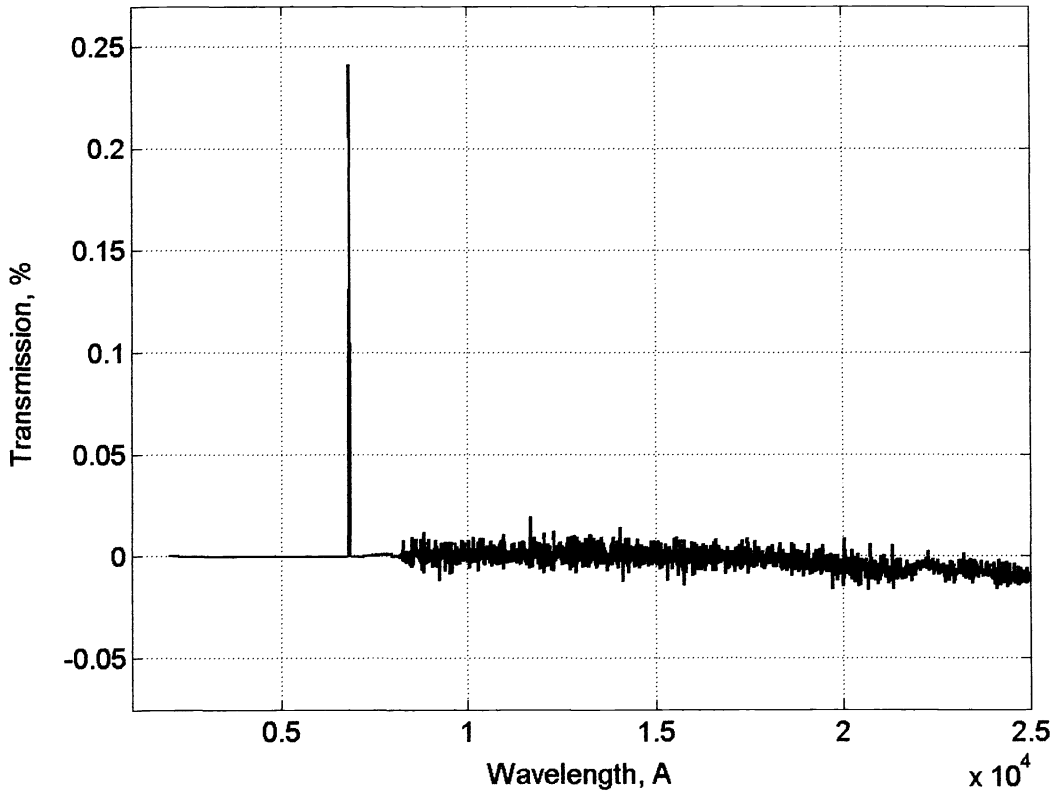

Fig. 1: Overall spectral performance of H-alpha system (including etalon and auxiliary filters) by Coronado [1].

Fig. 2: An example of an air-spaced front-end etalon-based H-alpha filter.

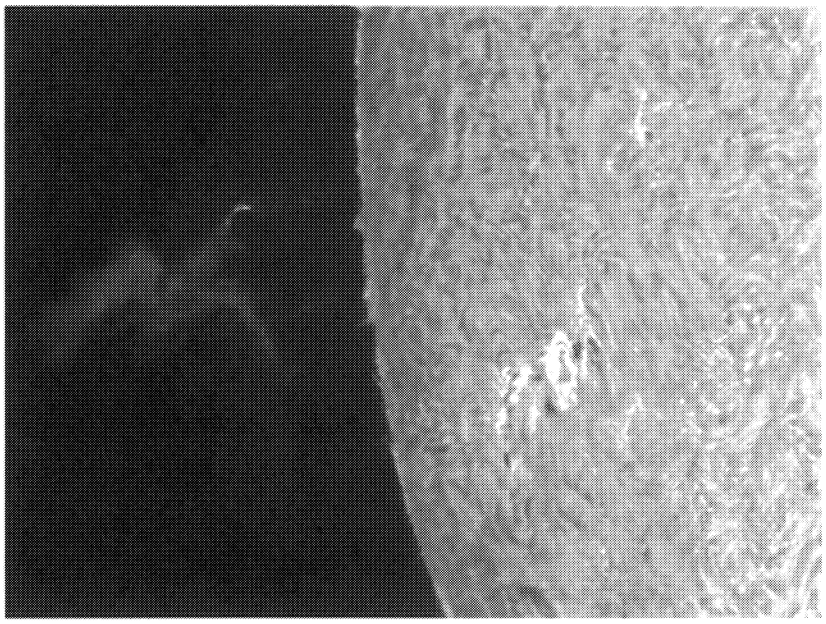

Fig. 3: Image of corona mass ejection and the Sun's chromosphere obtained with SolarMax60™ (courtesy of Jack Newton, [3]).

The defect finesse is an overall measure of the deviation of the etalon from perfection. In terms of microscopic etalon parameters F_D is defined by deviation of the etalon plates from planar reference (δ_S), deviation of the mirror surfaces from being truly parallel (δ_p), and the plate rms roughness (δ_{rms}), and is approximately given by [7]

$$F_D = \frac{\lambda}{\sqrt{4\delta_s^2 + 22\delta_{rms}^2 + 3\delta_p^2}} \qquad (4)$$

In practice, it is the defect finesse that sets an upper limit to the spectral resolution possible with a given etalon; in addition, the broadening of etalon's pass-band also implies a decrease in the peak transmittance (as a smaller-order effect).

a) While providing for required pass-band of < 0.7 A when observing the Sun in H-alpha, for example, the effective finesse of about 18 can be realized in a commercially reliable and mass-producible design. Typically, then, the reflectance finesse would be about 20, which in turn defines F_D in excess of at least 25 (see Fig 4). The surface flatness of $\lambda/50$ or better (at $\lambda = 6563\,\overset{o}{A}$) and surface micro-roughness of about a nm or less, which are routinely achieved in etalon fabrication of etalons by using continuous ring polishing technique allow us to achieve the adequate defect finesse (see Fig. 6). "Continuous" means that the part is always in intimate contact with the lap, while "ring" refers to the geometry of the lap. (Using this conventional technique is also known to produce Fabry-Perot plates in the one two-hundredth wave class of flatness.)

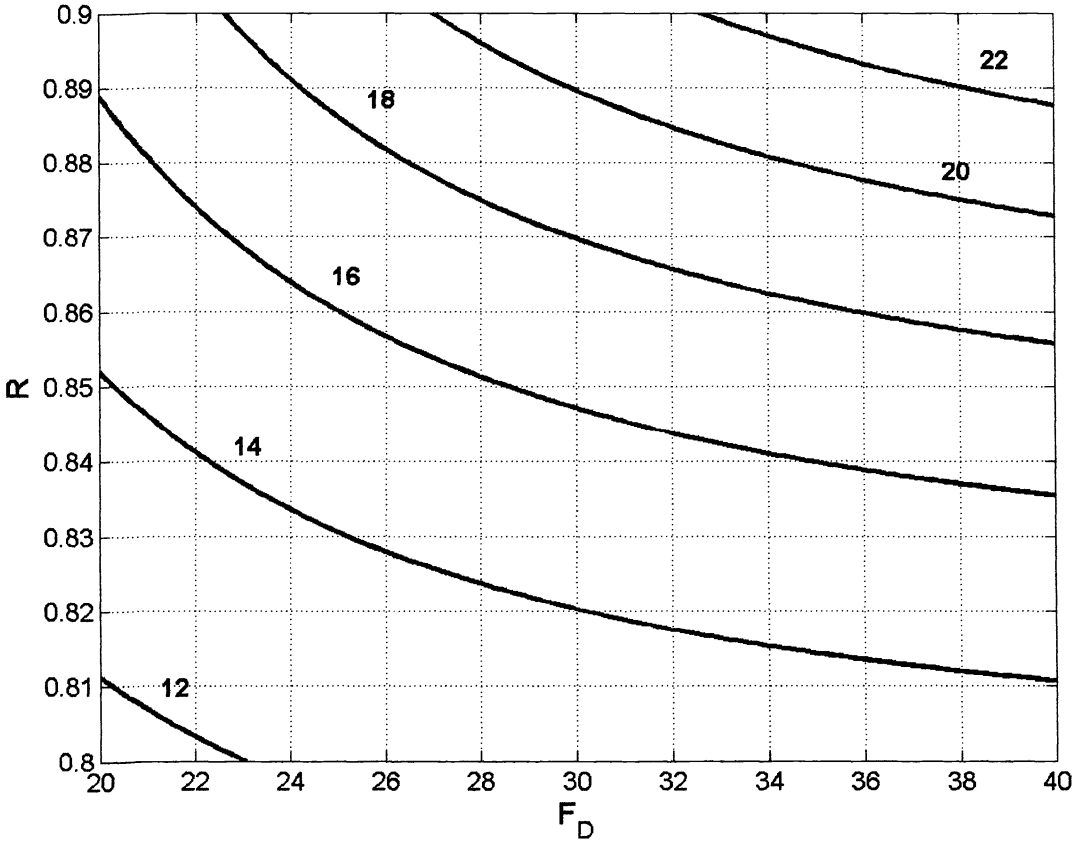

Fig. 4: Contour plot, presenting effective finesse of FPE as a function of its defect finesse and mirror reflectances.

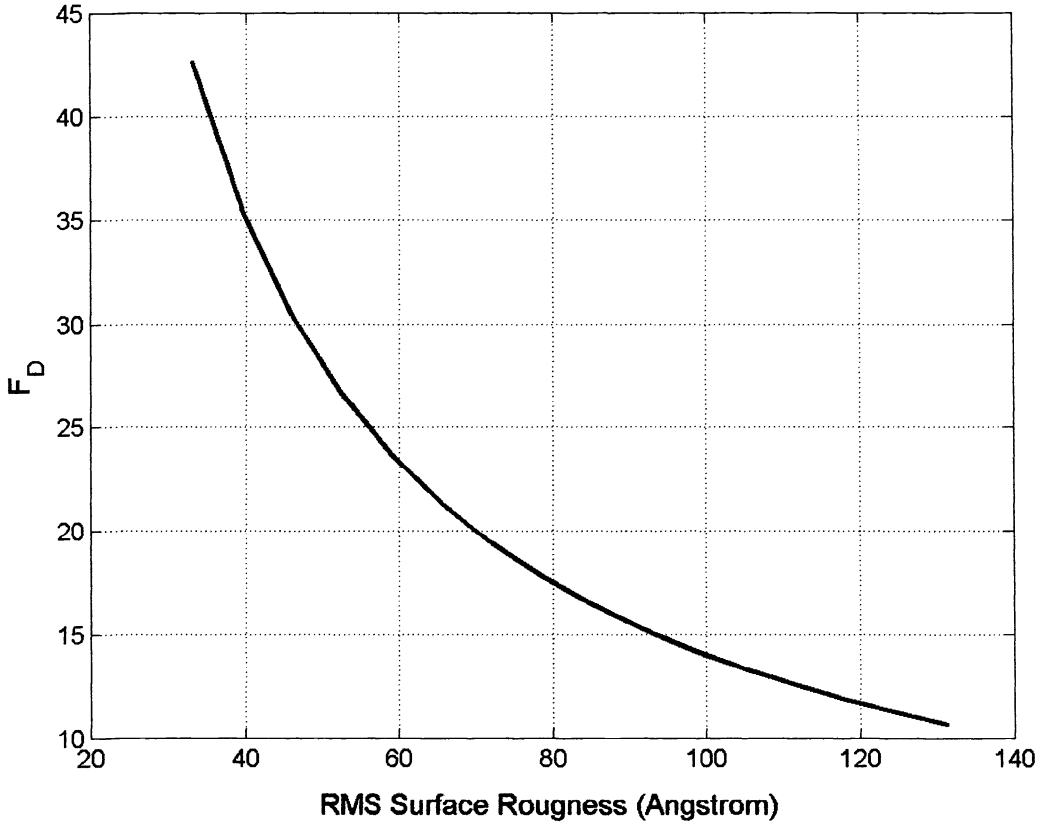

Fig. 5: Defect finesse vs rms surface micro-roughness of FPE mirrors (assumes parallel and flat etalon plates).

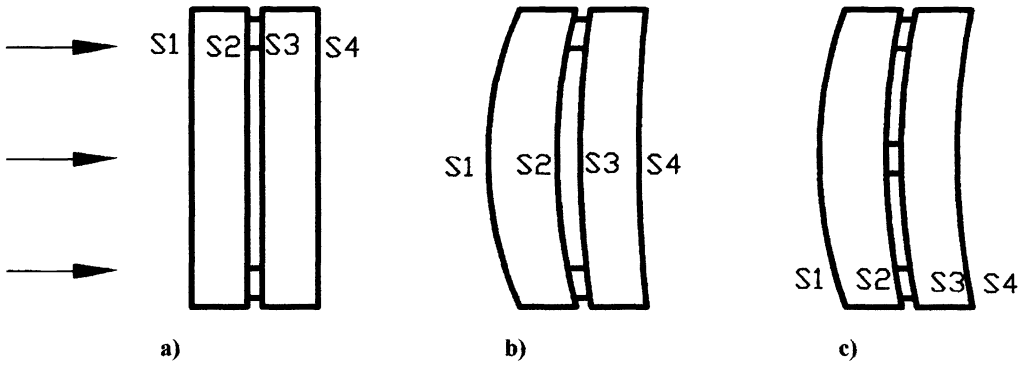

Fig. 7: Extortions of the shape of the etalon exposed to heat.

b) The deviation-from-parallelism error, δ_p, cannot be conventionally achieved without actively influencing the etalon gap (though temperature control and use of piezo-electric tuning elements, for example, [8]). The major reason for that is the temperature change that the solar filter has to experience during its performance, which inevitably leads to deviations from the ideal shape even for perfectly constructed air-spaced etalon. Indeed, for a classical air-spaced etalon, characterized by a certain bandwidth (FWHM) and a tuned central wavelength (CWL) at temperature T, if the temperature is changed to T_1, the etalon will have the same FWHM and CWL only once the etalon has come into thermal equilibrium at the new temperature, but not while it's changing its temperature. This is an important practical limitation on using such an etalon as a solar filter because, as the filter is facing the Sun during use, the filter is never in thermal equilibrium.

To resolve this problem, we developed a new approach to construction of air-spaced etalons, which incorporates the increasing the number of edge spacers and adding an extra spacer in the center [9]. This technology not only improves the ability to manufacture such etalons economically and in quantities, but also dramatically improves their thermal stability under non-thermal equilibrium conditions, as will be understood from the following discussion (design and optical performance details will be addressed elsewhere).

Fig.7A represents an air-spaced etalon with edge spacers only. Radiation from the Sun is incident on the fused-silica front surface S_1 of the etalon, thus raising the temperature after a time t to T_1. (In some cases there will be an energy rejection filter (ERF) positioned in front of the etalon; however, due to this component's absorbing a high percentage of the incident radiation, the temperature of the ERF will increase and the ERF will, in turn, become the heat source for the etalon). Due to the poor thermal conductivity of the fused silica, the temperature at surface S_2 is somewhat lower, T_2. The same argument applies to S_3 and S_4. Thus, the temperatures at these surfaces at any time t are related by $T_1 > T_2 > T_3 > T_4$; hence, the lateral expansion of the etalon plates is different at each surface (and every plane in between). Because the plates are conventionally rigidly held together at the edges by the spacers, this situation results in the shape depicted in Fig. 7B: the air-space between the plates takes on the shape of a meniscus gap instead of a plane parallel gap required of the etalon. The central wavelength is caused to change in accordance with the new 'average' thickness of the gap and the bandwidth of the etalon to broaden due to the gap no longer being parallel. In Fig. 7C can be seen the result of adding a central spacer to an etalon undergoing the same thermal radiation. In this case, as the first etalon plate bends under the influence of the thermal gradient, the central spacer ensures that the second plate bends in the same manner, even though this bending would normally be less under the incident thermal load. The result is that both the thickness of the air-gap and the parallelism of the surfaces S_2 and S_3 are maintained to a high degree of accuracy.

4. TEMPERATURE TUNABILITY OF ETALON BASED SOLAR FILTERS

The effects of change of ambient temperature on etalon's performance, such as free spectral range (FSR) and peak wavelength are defined by temperature-dependent material and optical characteristics of materials used in etalon's construction. Specifically, the (non-zero) coefficient of thermal expansion (CTE, α) of the spacers for air-spaced etalon and CTE and thermal dispersion of refractive index (dn/dT, β) of the spacer layer for solid etalon affect the degree of these etalons' thermal stability and allow for some temperature-defined spectral tuning of the peak wavelength via the temperature dependent change of optical length of the cavity, ΔD, according to

$$\frac{\partial(\Delta D)}{\partial T} = \sum_i d_i \left[n_i + (\beta_i + \alpha_i n_i) \right] \qquad (5)$$

It is advantageous to use solid-spaced etalons for applications requiring spectral tunability, such as atmospheric measurements. In [4] we demonstrated temperature tuning of the etalon constructed from Cleartran™ over a complete free spectral range with only ~20° C temperature change. In addition to temperature tunability, solid-spaced etalons

provide wider angular acceptance (proportional to the effective refractive index of the etalon cavity), as compared to air-spaced etalons, thus reducing the clear aperture requirements.

5. MULTI-STACKING OF ETALONS

To use an etalon as a narrow-band filter, the input light must be nearly collimated: the maximum angle $\theta_{inc,\max}$ of the input cone of light depends on the ability of the system to tolerate the degradation in optical performance, and is conveniently referenced to be

$$\theta_{inc,\max} < \sqrt{\frac{\lambda}{dF_E}} \qquad (6)$$

A single-etalon filter performance, however, is not always sufficient. To increase contrast ()effectively, signal-to-noise ratio) of the observed features a known "double-stacking" (i.e., a tandem of two) of the etalons can be employed. Such an operation narrows the band down to < 0.5 A. (Some solar background filters for lidars occasionally require triple-stacking of etalons [10]). When forming the tandem of etalon filters for direct solar observing we found it useful to fabricate otherwise identical constituent etalons as detuned from one another. In practice this allows bringing them both on line with a small angular tilt. This simple approach to forming a double-stacked system helps compensating the unequal detuning of filters due to variable conditions of operation (such as ranging temperature and barometric pressure) and removing the unwanted "image ghosts" due to residual retro-reflections within the optical system.

6. ACKNOWLEDGEMENTS

The authors would like to thank everyone on the team of Coronado Technology Group for development of solar filters, and Dr. B. Ralph Chou (University of Waterloo, Waterloo, Ontario, Canada) for providing independent measurements of their spectral characteristics.

7. REFERENCES

[1] www.coronadofilters.com
[2] C. Denker et al, "IRIM – an imaging magnetograph for high-resolution solar observations in the near-infrared", Proc. SPIE, v. 4853.
[3] N. H. Zaun, C. Weimer, D. Lunt, and Y. Sidorin, SPIE Annual Meeting, Proc. SPIE, v. 5542, paper # 5542-18, *to be published* (SPIE annual meeting 2004).
[4] Y. Sidorin, D. Lunt, M.A. Krainak, M.A. Stephen, A.J. Martino, R.S. Lancaster, and Graham R. Allan, Proc. SPIE, v. 5542, paper # 5542-17, *to be published* (SPIE annual meeting, 2004)
[5] H.A. Macleod, *Thin Film Optical Filters*, McGraw-Hill, 1989.
[6] courtesy of Jack Newton, www.jacknewton.com ; taken with a SolarMax™ 60 solar filter.
[7] P.D. Atherton, N.K. Reay, J. Ping, and T.R. Hicks, *Opt. Eng.*, 20, 806-814, 1981.
[8] W.R. Skinner, P.B. Hays, H.J. Grassl, D.A. Gell, M.D. Burrage, A.R. Marshall, and J. Kafkalidis, Proc. SPIE, 2830, 202-214, 1996.
[9] D. Lunt, US Pat. #6,181,726.
[10] J.A. McKay, *Appl. Opt.*, 38, 5851-5858, 1999.